Exercise modulates human hippocampal-cortical ripple dynamics

Araceli R. Cardenas[1]†, Juan F. Ramirez-Villegas[2]†, Christopher K. Kovach[3], Phillip E. Gander[4], Rachel C. Cole[5], Andrew J. Grossbach[6], Hiroto Kawasaki[3], Jeremy D.W. Greenlee[3], Mathew A. Howard III[3], Kirill V. Nourski[3,7], Matthew I. Banks[8,9], Michelle W. Voss[7,10,11]*

[1] Krembil Brain Institute, Toronto Western Hospital, University Health Network, Canada

[2] Institute of Science and Technology Austria (ISTA), Am Campus 1, Klosterneuburg 3400, Austria

[3] Department of Neurosurgery, The University of Iowa; Iowa City, IA, United States

[4] Department of Radiology, The University of Iowa; Iowa City, IA, United States

[5] Department of Neurology, The University of Iowa; Iowa City, IA, United States

[6] Department of Neurosurgery, Ohio State University; Columbus, Ohio, United States

[7] Iowa Neuroscience Institute, University of Iowa; Iowa City, IA, United States

[8] Department of Anesthesiology, University of Wisconsin School of Medicine and Public Health; Madison, WI, United States

[9] Department of Neuroscience, University of Wisconsin School of Medicine and Public Health; Madison, WI, United States

[10] Department of Psychological and Brain Sciences, University of Iowa; Iowa City, IA, United States

[11] Interdisciplinary Graduate Program in Neuroscience, University of Iowa; Iowa City, IA, United States

†A.R.C. and J.F.R.V. contributed equally to this work

*Corresponding author: michelle-voss@uiowa.edu

Abstract

Physical exercise acutely improves hippocampal-based learning and memory in rodents and humans. While animal studies have mainly offered cellular- and synaptic-level accounts of these effects, human neuroimaging studies show that exercise improves hippocampal-cortical connectivity at the macroscale level. However, the neurophysiological basis for exercise-induced effects on human hippocampal-cortical circuits remains unknown. A growing body of evidence supports the critical role of hippocampal sharp wave-ripples (SWRs) in learning and memory. Moreover, recent studies suggest that the coupling between ripples in the hippocampus and neocortex reflect acute modulations in inter-regional connectivity required by mnemonic processes. Here, we examine the hypothesis that exercise modulates hippocampal SWR events and their coupling with ripples in other cortical areas. We performed intracranial recordings in neurosurgery patients during awake resting state, before and after one session of aerobic exercise. Exercise elicited an increase in ripple rate and duration in mesio-temporal areas (hippocampus, amygdala and parahippocampal gyrus). These changes in ripple features were also observed in the limbic and the default mode (DMN) networks. Furthermore, after exercise, we observed an increase in coupling and phase synchrony between ripples in these two networks and hippocampal SWRs. Our results elucidate the potential mechanisms by which aerobic exercise elicits its reported short-term effects in cognition. Further investigations are needed to explore how these exercise-induced acute modulations contribute to long-term changes in neural plasticity.

Significance Statement

Physical activity is a modifiable lifestyle factor that improves cognitive function and prevents age-related cognitive decline. Even one session of exercise can enhance hippocampal-based memory and learning. However, the neurophysiological mechanisms by which exercise acutely affects human cognition remain unknown. Using intracranial recordings in neurosurgical patients we show that the hippocampus and neocortex often synchronize their activities via high-frequency neural synchrony events known as ripples.

After exercise, hippocampal and neocortical ripples were prolonged and emerged more frequently. Moreover, hippocampal and neocortical ripples exhibited increased coupling and phase synchrony. These effects were neocortical region-specific, favoring structures of the limbic and default mode networks. Ultimately, our results shed light on the mechanisms behind the preventive and therapeutic potential of exercise interventions.

Introduction

Physical exercise improves memory and learning in rodents and humans (*1*, *2*). Recent data highlight the importance of hippocampal circuits to these cognitive benefits (*3*, *4*). Animal studies have focused on the molecular, histological and endocrine mechanisms by which exercise drives synaptic plasticity and neurogenesis in the hippocampus (*5*–*7*). In contrast, human neuroimaging studies have shown that exercise increases hippocampal-cortical functional connectivity both acutely (*8*, *9*) and after months of training (*4*, *10*, *11*). However, human data available to date relies exclusively on hemodynamic measures and cannot speak to the neurophysiological mechanisms supporting exercise-induced changes in connectivity and ultimately cognition.

There is a growing understanding of the neurophysiological mechanisms supporting hippocampal-based learning and memory (*12*). For instance, during periods of quiescence or non-rapid-eye-movement (NREM) sleep, slow field potential deflections accompanied by high frequency oscillations (HFOs), known as sharp wave-ripple (SWR) complexes, occur in the hippocampus and play a critical role in memory consolidation (*13*, *14*). Occurrence of hippocampal SWR is linked to widespread patterns of cortical activation and simultaneous subcortical deactivation (*15*, *16*). Furthermore, the occurrence of ripples in the neocortex (*17*) and their functional role (*18*–*20*) has gained attention. In both rodents and humans, the coupling between hippocampal and neocortical ripples has been functionally associated with memory retrieval and learning (*18*, *20*). Recent evidence indicates that ripple coupling is a neurophysiological marker of transient, short-term functional connectivity(*21*).

In this work, we obtained intracranial electroencephalographic (iEEG) recordings in neurosurgical patients during awake resting state, before and acutely after exercise. Our central hypothesis was that exercise would acutely modify ripple dynamics in the mesial temporal lobe and increase hippocampal-cortical interactions in the ripple band of local field potentials (LFPs). We found that exercise modulates ripple rate and properties (duration and peak frequency) broadly across the medial temporal lobe including the hippocampus (HC), amygdala (AMY), and parahippocampal gyrus (PHG). Notably, exercise changed ripple-associated hippocampal connectivity with the limbic and default mode network (DMN), as evidenced by enhanced ripple coupling and synchrony. Overall, our results show that exercise modulates hippocampal-cortical ripple dynamics, introducing a new putative mechanism by which physical activity could enhance memory and learning.

Participants (N=14, 10 males) were neurosurgical patients being monitored for epileptic seizure localization with chronic intracranial electroencephalography (iEEG) recordings. Patients completed an acute exercise paradigm while neural activity was continuously monitored. The paradigm consisted of a pre-exercise resting state period (~20 min), followed by a period of guided exercise on a pedal exerciser (~20 min), and then by a post-exercise resting state period (~20 min) (Fig. 1A). During resting periods, participants were instructed to relax with their eyes closed. During exercise, participants started with a warm-up (~5 min), and then cycled at a target range of light-to-moderate intensity aerobic exercise [50-60% of their age-predicted maximum heart rate (HR%)]. Participant demographics and physiological response to exercise are summarized in **Table S1**. On average, participants (median age = 23.5, range 17 to 50) were physically active with an average of 7.6 hours (SD=3, min-max 3-14) of self-reported non-sedentary physical activity per day. Compliance to the exercise protocol was satisfactory, with an average HR% during exercise of 57.7% (SD=5.7), with most participants within or near the target range and as a group were elevated compared to the pre-exercise rest ($t(12)=7.12$, $p<0.001$; Fig. 1A). Similarly, self-reported RPE was an average of 11.9 (SD=1.5), corresponding to a subjective intensity of “light” to “somewhat hard” on the scale matching their target intensity zone, and was significantly elevated compared to the pre-exercise

rest ($t(11)=7.57$, $p<0.001$). Age, sex, and self-reported physical activity were not correlated with acute exercise intensity (p's all >.05), and therefore were not entered as covariates in analyses reported in this study.

Electrode coverage across patients is summarized in Fig. 1B. Signals from 2415 recording sites were collected from the 14 patients included. Cortical coverage encompassed frontal, parietal, temporal, and occipital cortices. Cortical recording sites were grouped into 7 canonical networks according to a previous study (*22*) (Fig. 1B, left sub-panel). Mesial coverage included hippocampus, parahippocampal gyrus, and amygdala (Fig. 1B, right sub-panel). Contacts out of the brain, in the seizure onset zone (SOZ), or exhibiting interictal epileptiform discharges (IEDs) during the recordings were removed from the analysis. Automated noise rejection and denoising steps were subsequently applied to the remaining signals (Materials and Methods). For ripple detection, LFP signals were bipolar-referenced to the nearest white-matter recording site. The findings described in the following sections result from the comparison between the pre- and post-exercise resting state periods, while subjects stayed quiescent, silent, and with closed eyes.

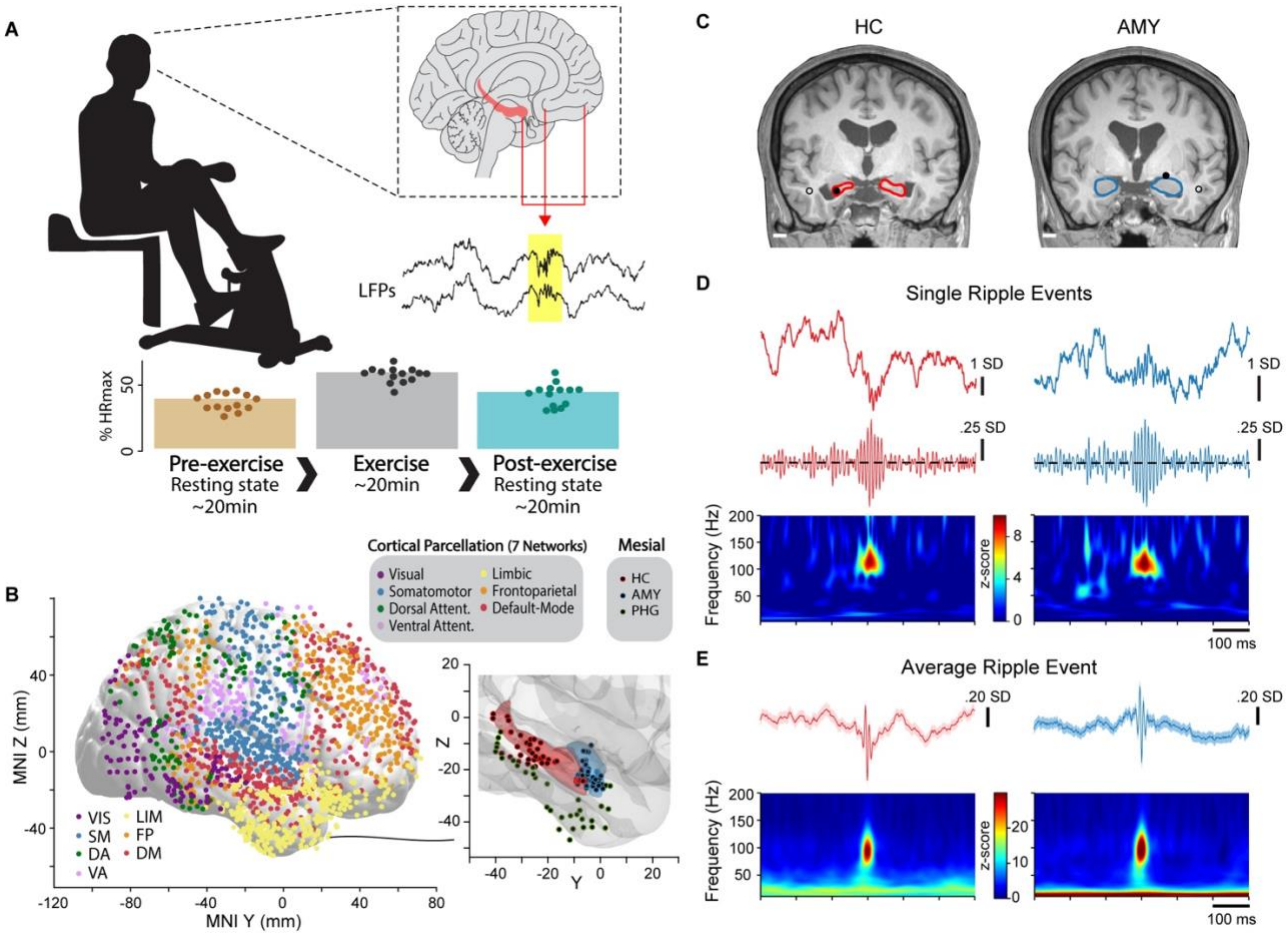

Fig. 1. Paradigm, electrode coverage and ripple detection. (A) Left: Illustration of the experimental paradigm. Neurosurgical patients (N = 14) were instructed to complete an acute exercise paradigm while intracranial EEG activity was continuously recorded. A pre-exercise resting period (~20 min), was followed by exercise on a mini-bike (~20 min), then followed by a postexercise resting period (~20 min). Right: pre-, during, and post-exercise heart rate (percentage of age-predicted maximum) showing that compliance to the acute exercise protocol was satisfactory (50-60% target range) across subjects (individual dots). *p<0.001 paired-samples t-test for the comparison between pre-exercise resting state HR% and exercise HR%. **(B)** Electrode coverage across participants. Left: Cortical electrode coverage. Cortical contacts were grouped into 7 canonical networks using the Yeo-parcellation according to their anatomical location, as indicated by colors (visual, somatomotor, dorsal attention, ventral attention, limbic, frontoparietal, and default-mode). Right: Electrode coverage in the hippocampus, amygdala and parahippocampal gyrus. **(C)** Two exemplary contacts (filled circles) located in hippocampus (left, red) and amygdala (right, blue) (outlined areas) are shown overlayed in anatomical MRI T1 images. For each structure, the nearest white matter contact (empty circles in the MRI image) was used for re-referencing. **(D)** Raw (<300 Hz) and filtered (70-160 Hz) LFPs (top/middle), together with the spectral decomposition of the raw LFP (bottom), show that ripple events can be reliably identified in the electrical activity of the hippocampus (left, red) and

amygdala (right, blue). **(E)** Top: Single-channel averaged peri-ripple LFP trace (<300 Hz); Bottom: Averaged z-scored peri-ripple spectrogram for hippocampus (left) and amygdala (right). Shading indicates standard error of the mean (SEM).

Acute exercise modulates ripple properties

Ripples were reliably identified in the LFP signals recorded from depth electrodes targeting HC (*18*, *19*), PHG (*23*, *24*), and AMY (*25*) (Fig. 1C-E). Briefly, these oscillatory events were detected as peaks exceeding 4 SD threshold in the z-scored envelope of the LFP signal filtered in the 70-160 Hz frequency range (Materials and Methods).

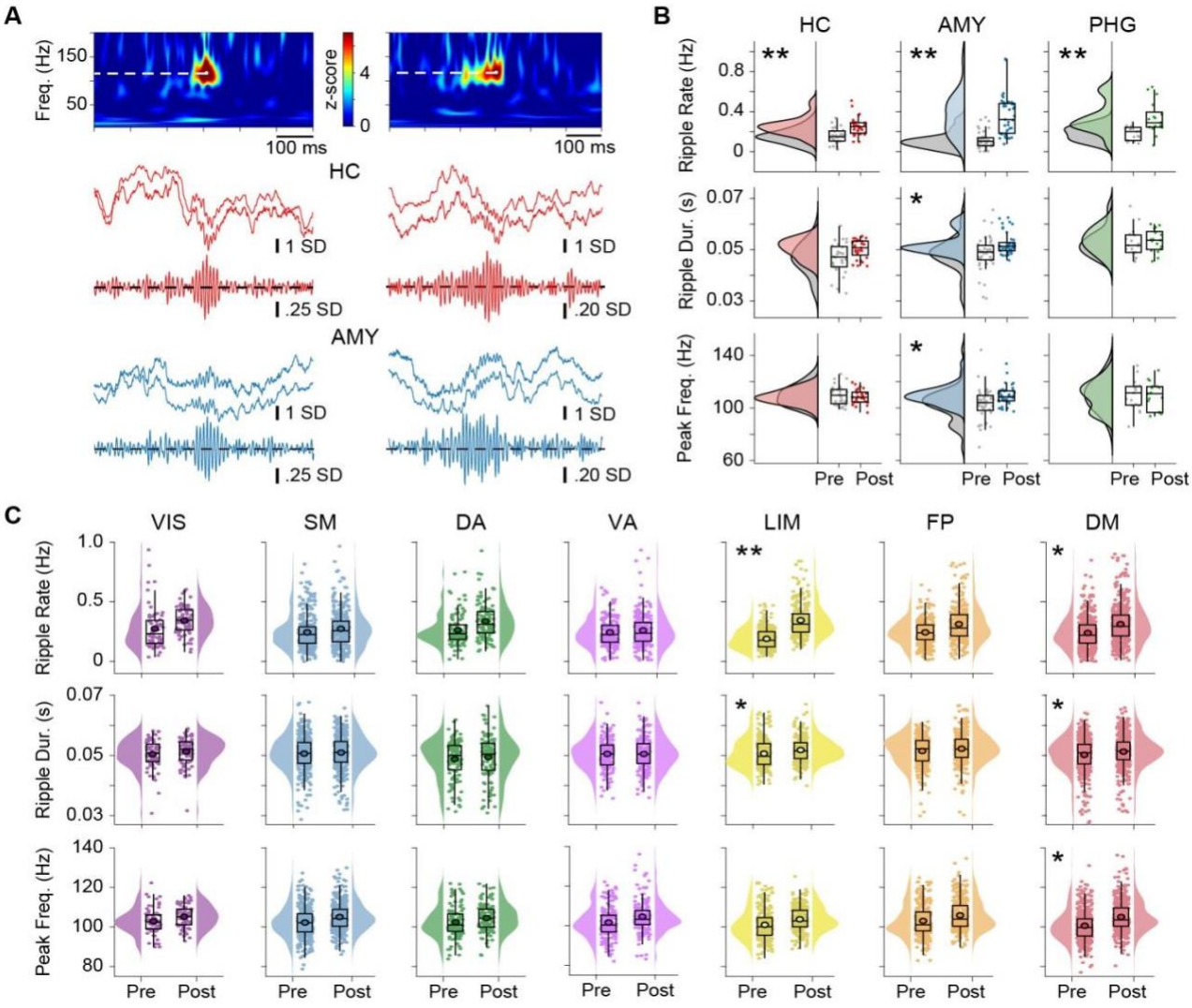

Fig. 2. Effect of acute exercise on ripple properties. (A) Exemplary raw (<300 Hz) and filtered (70-160 Hz) peri-ripple LFP traces with spectrograms showing that ripples in the human hippocampus and amygdala vary in duration and peak frequency. White, dotted lines in the spectrograms indicate ripple frequency peak at time zero. Two traces of the raw LFP per anatomical structure are displayed to show the variability across contiguous sites. **(B)** Across-subjects distributions of ripple rate, duration and peak frequency per site in the resting state pre- and post-exercise in mesial temporal areas (HC, AMY and PHG), and **(C)** in the 7 canonical networks, illustrating the modulation of ripple characteristics by acute exercise. In box plots, lines crossing the boxes indicate the median, box edges indicate 25th and 75th percentiles, and data points beyond the whiskers are outliers. Each dot represents one recording site. *p<0.05, **p<0.01 according to a LME model treating subject and recording sites as random effects.

The rate of hippocampal ripples and their electrophysiological features are known to vary across behavioral states and to predict memory performance (*26*, *27*). We hypothesized that exercise would be associated with an increase in ripple occurrence and modulation of ripple electrophysiological features in mesial temporal areas. To this end, we computed the ripple rate per channel in the pre- and post-exercise periods. Group-level statistical comparison between the pre- and post-exercise resting state blocks was performed using a linear mixed effects model (LMEM) with ripple rate as the dependent variable. Condition (pre- and post-exercise) over each anatomical region were treated as within-subjects fixed effects. Subject and recording sites were included as random effects to account for differences in electrode coverage across patients (Materials and Methods). We found significant pre-to-post exercise ripple rate increases for hippocampus (b=0.06, SE=0.02, t(170)=3.02, *p*=0.002), amygdala (b=0.98, SE=0.19, t(170)=4.98, *p*=0.00000151), and PHG (b = 0.58, SE=0.02, t(170)=2.55, *p*=0.011) (Fig. 2B, top row).

Fig. 2A shows exemplary raw traces of peri-ripple LFP of hippocampus and amygdala, where variability in duration and power spectral density are apparent. To investigate whether exercise modulates these electrophysiological features, a LMEM analogous to the one previously described was deployed per feature by changing the dependent neural variable (Materials and Methods). We found that ripple duration and peak frequency increased from pre- to post-exercise for the amygdala (duration: b=0.00156, SE=0.000743, t(170)=2.11, *p*=0.036; peak frequency: b=2.89, SE=0.98, t(170)=2.94,

p=0.0036; Fig. 2B). In contrast, exercise did not significantly affect ripple duration or peak frequency in the HC or PHG.

In light of these observations, we investigated whether the electrophysiological features of ripple events were also modulated in the rest of the brain as a putative consequence of acute physical activity. To examine this possibility, after ripple detection and feature computation, cortical sites were grouped according to seven canonical networks (*22*). Between-subjects statistical analysis was again performed using the same LMEM, which treated subjects and recording sites as random effects. Consistent with our previous results, exercise increased ripple event rate and duration in the limbic network (rate: b=0.065, SE=0.014, t(3330)= 4.59, *p*=0.00000441; duration: b=0.000545, SE=0.000256, t(3327)=2.12, *p*=0.0000426; Fig. 2C). Notably, the DMN exhibited significant exercise-related increases in ripple rate, duration and peak frequency (rate: b=0.030, SE=0.013, t(3330)=2.23, *p*=0.025; duration: b=0.00047, SE=0.00023, t(3327)=1.99, *p*=0.045; peak frequency: b=1.84, SE=0.87, t(3327)=2.11, *p*=0.034). The interaction of pre- and post-exercise blocks with the rest of the canonical networks remained non-significant for the studied ripple features (*p*>0.05; Fig. 2C). These results indicate that acute exercise elicits an increase in the rate of ripple events and modulates their properties (duration and peak frequency) in limbic areas and the DMN. Next, we explore whether such local effects are accompanied by an increase in hippocampal-neocortical interactions.

Acute exercise increases hippocampal-cortical ripple coupling

Ripples in mesial areas often co-occurred with similar short-lived high-frequency events in other brain areas during pre- and post-exercise resting state (exemplary event seen across cortical areas is shown in Fig. 3A). To test whether exercise modulates ripple hippocampal-cortical coupling, we performed cross-correlation analysis between the time stamps of ripples in the hippocampus (anchor events) and other sub-cortical and cortical sites (Fig. 3B; Materials and Methods). To this end, we paired one hippocampal recording site per subject (selected based on its anatomical location) with the other sites of interest. To guarantee an unbiased coupling estimate, cross-correlation values per pair were

corrected for potential ripple-rate baseline effects by subtracting baseline values obtained by a permutation procedure (Fig. 3B; Materials and Methods). Fig. 3C shows pre and post peri-event correlation values in exemplary hippocampo-cortical pairs. As in the previous section, the influence of exercise in hippocampal-cortical ripple coupling across subjects was tested using a LMEM. In this case, the dependent variable was average coupling measured around ripple occurrence in the hippocampus (Materials and Methods).

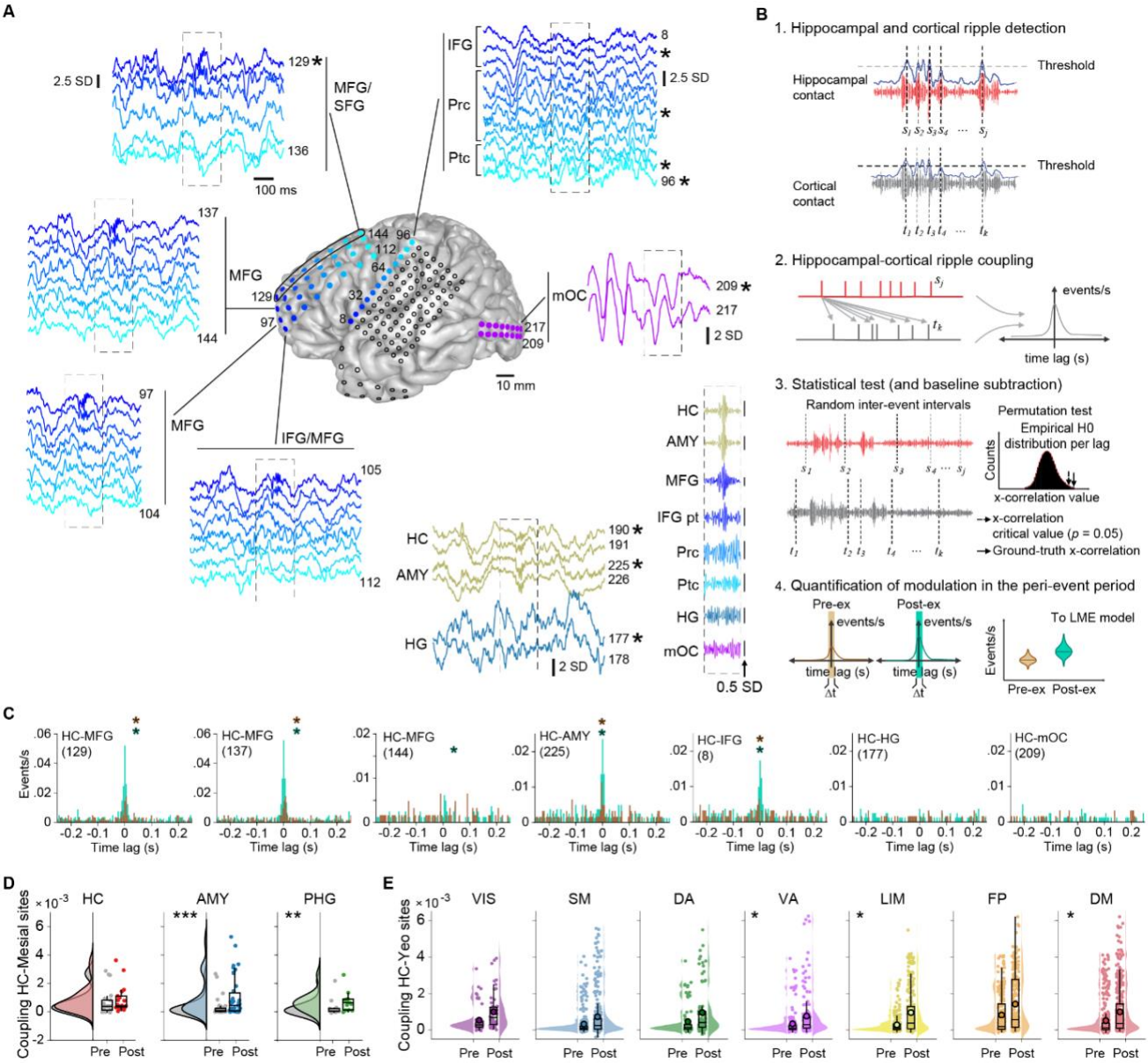

Fig. 3. Effect of exercise on hippocampal-cortical peri-ripple coupling. (A) Raw (<300 Hz) LFP traces, showing the coupling between a hippocampal ripple and similar high-frequency events occurring in the amygdala and associative cortical areas, but not in sensory areas (shown in the bottom 70-160Hz filtered

traces; Prc: precentral gyrus; Ptc: postcentral gyrus; IFG pt: inferior frontal gyrus, pars triangularis). **(B)** For the peri-ripple coupling calculation, ripples are first detected in the hippocampus and neocortex, represented by the variables *s* and *t*, respectively. A cross-correlation is computed using these two point-processes (i.e. a histogram of the *time lags* or differences between ripple occurrence times; see Materials and Methods). (3) Statistical significance for the correlation values is computed with respect to a null-hypothesis distribution of cross-correlations calculated from random point processes of the same rate. (4) The coupling is then computed as the averaged cross-correlation in a time window of +/- 250 ms around zero lag. **(C)** Exemplary cross-correlograms between hippocampal ripples and ripples from distinct extra-hippocampal sites (MFG: middle frontal gyrus; AMY: amygdala; IFG: inferior frontal gyrus; HG: Heschl's gyrus; mOC: middle occipital gyrus). Asterisks indicate significant coupling around lag zero (p<0.01). **(D)** Across-subjects pre- and post-exercise resting state coupling values between hippocampal ripples and ripples detected in other mesial areas (i.e., HC, AMY, and PHG). **(E)** Across-subjects pre- and post-exercise resting state coupling values between hippocampal ripples and ripples detected across 7 canonical networks: visual, somatomotor, dorsal attention, ventral attention, limbic, frontoparietal and default-mode. **(D and E)** LME models for the comparison between pre- and post-exercise resting state blocks. In box plots, lines crossing the boxes indicate the median, box edges indicate 25th and 75th percentiles, and data points beyond the whiskers are outliers. *p<0.05, ** p<0.001.

Group-level LMEM-based analysis (Fig. 3E) shows that, after exercise, ripple coupling increases predominantly between the hippocampus and the limbic network, and between the hippocampus and DMN (limbic: b=0.000242, SE=0.000103, t(2752)=2.34, p=0.019; DMN: b= 0.000231, SE=0.000102, t(2752)=2.26, p=0.023). The ventral-attention network exhibits enhancement in coupling with hippocampal ripples that reached statistical significance (b=0.000219, SE=0.000104, t(2752)=2.09, p=0.035). In contrast, the effect was not significant in the other four networks (visual, somatomotor, dorsal-attention and frontoparietal, p>0.05). These results were consistent across peri-ripple windows of different lengths, confirming the robustness of the effect in the limbic and default-mode networks. Thus, hippocampal ripples selectively co-occur with ripples in these networks, and this coupling is larger during post-exercise resting state, as compared to pre-exercise resting state.

Using the previous approach, we also explored whether exercise modulated ripple coupling between different mesial areas of interest (Fig. 3D). We found that exercise significantly increased hippocampal-amygdala (b=0.000342, SE=0.0000878e,

t(144)=3.89, *p*=0.00015) and hippocampal-PHG ripple coupling (b=0.000296, SE=0.000106, t(144)=2.78, *p*=0.006). Altogether, our results indicate that exercise not only modulates local ripple properties, but also enhances mesio-neocortical and intra-mesial ripple coupling.

Hippocampal-cortical ripple phase synchrony is enhanced by exercise

Recent studies have shown that high frequency oscillations are synchronized between distributed brain regions and reliably exhibit a network organization (*20*, *21*). As ripples are a manifestation of volleys of spiking neurons, ripples (and hence population spike discharges) may be phase-locked across distinct, yet functionally connected brain areas. Given the increase in ripple coupling we observed after exercise, we explored whether exercise also modulated ripple phase synchronization.

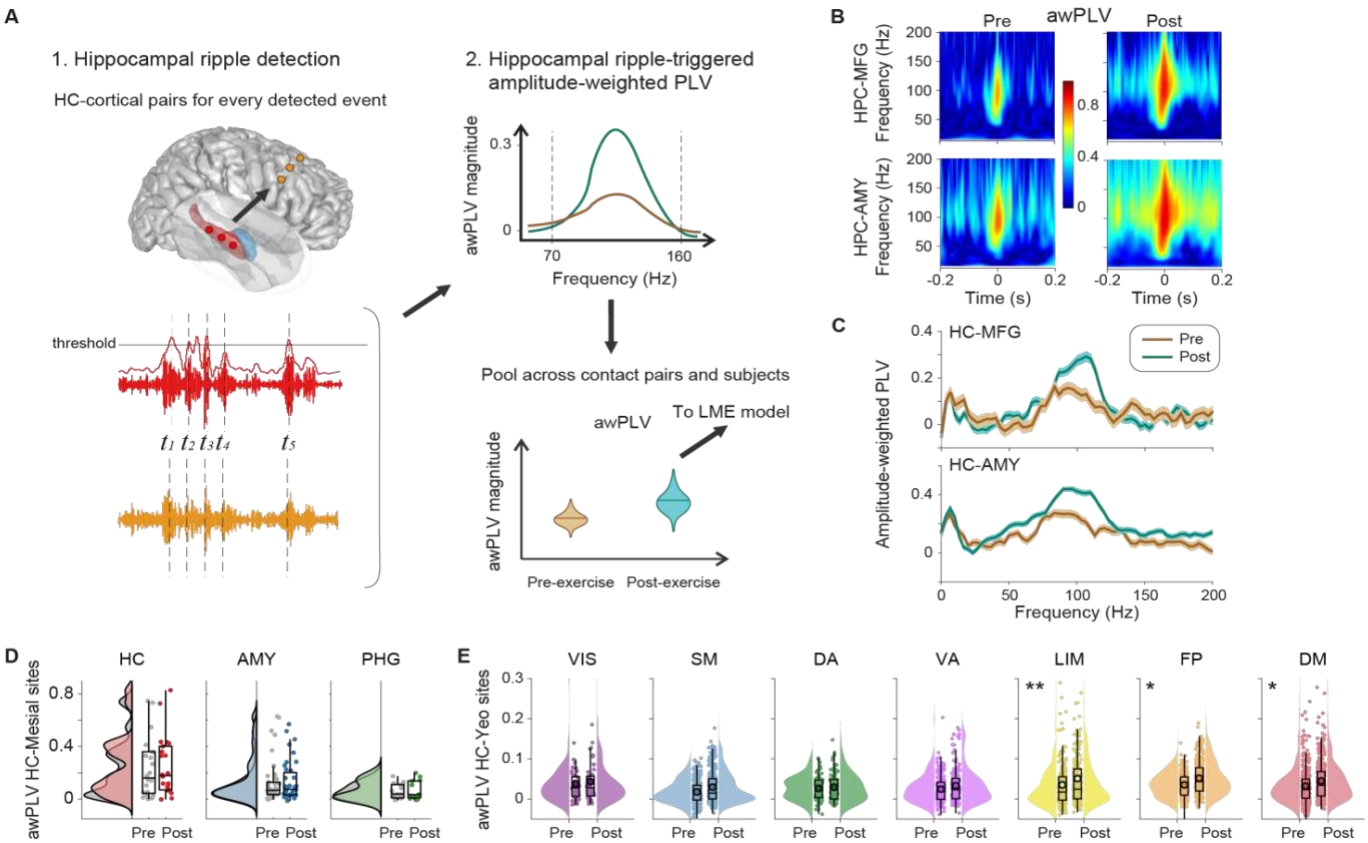

Fig. 4. Effect of exercise on hippocampal-cortical peri-ripple phase synchrony. (A) For phase synchrony calculation, hippocampal ripple time stamps used to compute a peri-event amplitude-weighted

phase locking value (awPLV) between hippocampal-cortical site pairs. The ripple band (70-160 Hz) averaged awPLV estimate per site pair is then used for group-level statistical analysis using a LMEM. **(B)** 2-D awPLV estimated from complex Morlet-wavelet spectrograms between the hippocampus and middle frontal gyrus (MFG) (top), and between the hippocampus and amygdala (bottom), shows that awPLV between hippocampus and other brain areas increases during post-exercise (right), relative to pre-exercise resting state (left). **(C)** Same as panel (B), but the awPLV estimate is 1-D and calculated via demodulated band transform (DBT). **(D)** Across-subjects pre- and post-exercise resting state awPLV at the time of hippocampal ripples between hippocampus and other mesial areas (i.e., HC, AMY, and PHG). **(E)** Across-subjects pre- and post-exercise resting state awPLV at the time of hippocampal ripples, between hippocampus and 7 canonical networks: visual, somatomotor, dorsal attention, ventral attention, limbic, frontoparietal and default-mode. **(D and E)** LME models for the comparison between pre- and post-exercise resting state blocks. In box plots, lines crossing the boxes indicate the median, box edges indicate 25th and 75th percentiles, and data points beyond the whiskers are outliers. *p<0.05, ** p<0.001.

To this end, the time stamps of ripples detected in the hippocampus were used as triggers to build peri-ripple LFP traces across all recorded sites. The phase synchrony between hippocampal and cortical ripples was measured by computing an amplitude-weighted phase-locking value (awPLV). Briefly, this quantity measures the degree to which two oscillatory signals are phase-locked, regardless of their amplitude (*28*) (Materials and Methods). Ripple-triggered awPLV responses were computed separately for pre-exercise and post-exercise resting state blocks in a ±250 ms window around the events' occurrence. Fig. 4B displays the averaged hippocampal-MFG and hippocampal-amygdala time-frequency awPLV for an exemplary subject (one MFG contact belonging to the DMN is shown). Notably, post-exercise peri-ripple awPLV was larger than its pre-exercise counterpart (Fig. 4B and C), indicating a higher ripple-band phase coupling of the former with respect to the latter.

The averaged awPLV in the ripple band (70-160 Hz) per channel pair was used for further statistical analysis across subjects (Fig 4A). Analogously to the former ripple coupling (cross-correlation) analysis, statistical comparison between pre- and post-exercise blocks over cortical areas was performed using a LME model to account for differences in subjects electrode coverage. The dependent variable of this analysis was the pre- and post-exercise awPLV (Methods). We found that the limbic, frontoparietal and DM

networks showed a significant effect for awPLV (Fig 4E; limbic: b=0.0085, SE=0.0027, t(2754)=3.11, *p*=0.001; frontoparietal: b=0.0062, SE=0.0027, t(2754)=2.24, *p*=0.024; DMN: b=0.0056, SE=0.0027, t(2754)=2.09, *p*=0.036). These results indicate that mesial and neocortical high-frequency ripples are phase locked, and this coupling is modulated by exercise in some networks but not others, with a robust effect in the limbic network.

In this investigation, we examined how acute exercise modulates mesial ripple properties and mesial-cortical ripple dynamics. We found that, after a session of acute exercise, ripples occur at higher rates and exhibit longer durations in mesial temporal areas, and the limbic and DM networks. We also quantified the coupling between ripples in the hippocampus and ripples in neocortical sites, before and after the exercise session. Whereas hippocampal and neocortical ripples were temporally- and phase-coupled in the pre-exercise period, physical activity enhanced the extent of this coupling, predominantly in the limbic and DM networks.

The rate of hippocampal ripples and their physiological features are known to vary across states and correlate with memory performance (*26*, *27*). For example, ripple duration increases as a result of mnemonically demanding situations, such as spatial learning (*26*). Moreover, animal models have revealed aging is associated with reduced ripple rate during sleep and awake resting state, which may contribute to age-associated memory impairment (*29*). In the context of these studies, the increase in ripple rate and duration acutely elicited by exercise in mesial areas may partially account for the beneficial effects of physical activity in cognitive function and age-related memory loss. Furthermore, our results contribute to the growing literature showing that ripple coupling is a widely distributed phenomenon. Ripples occur simultaneously and phase-lock across multiple brain regions, even between hemispheres (*21*, *30*). However, across-subject comparisons of the pre- and post-exercise epochs pointed to the limbic network and the DMN as important targets of the exercise intervention.

A multitude of studies have shown that the functional interactions between the hippocampus and neocortical regions play an important role in long-term memory,

learning, working memory, and decision making (*31–33*). Furthermore, the hippocampus and other mesial areas are functionally and anatomically connected with cortical areas, including structures of the limbic network (e.g. inferotemporal, orbital gyri) (*33–35*) and associative cortical areas (*15*, *20*, *22*, *36*). Hippocampal activity may propagate to distinct neocortical targets following excitation of the output layers of the entorhinal cortex (EC) (*37*), and/or via retrosplenial cortex (*38*). Furthermore, EC and neocortical activity may also modulate mesial activity across several brain states (*35*, *39–42*). In these scenarios, ripple coupling across distinct brain areas may reflect processing of mnemonic information, e.g., memory reactivation, transfer, or consolidation. Our results suggest these ripple-mediated memory functions may be further enhanced immediately following physical exercise.

The DMN is classically considered a resting-state network that supports inwardly oriented attention during episodic memory and future planning, as opposed to sensory-driven processing. In humans, the strongest ripple-coupled activations during autobiographic mnemonic recollection were found in the DMN (*19*). During resting state, the DMN may play a role in the propagation of replay by mediating hippocampal-neocortical interactions. For instance, endogenous resting state DMN fluctuations detected in BOLD-fMRI correlate with the occurrence of hippocampal ripples in anesthetized primates (*15*, *16*, *43*). Furthermore, in the off-line resting period of a memory task in humans, replay sequences thought to be packaged into bursts occurring during activation of the DMN and frontoparietal network (*44*). It has been hypothesized that the DMN could trigger HFO cascades spreading the reactivation of mnemonic and other representational content (e.g. semantic) (*31*). Altogether, this evidence advances a view of the DMN as a central hub in a bursting network (high synchrony neural events) that spreads information, possibly as “replay”, across broad cortical areas (*19*, *21*, *31*, *44*).

Whereas the results of this study suggest that the modulation of ripple dynamics is a mechanism by which exercise affects cognitive function, it is also possible that the observed changes reflect metabolic changes triggered by exercise. In rats, hippocampal ripples have been shown to modulate serum interstitial glucose changes (*45*). However,

the cognitive and metabolic roles of ripple dynamics are not mutually exclusive. Further experiments are required to disentangle how the metabolic changes triggered by exercise account for the observed ripple changes, and whether they intermingle with exercise acute effects on cognitive performance.

Acknowledgments: We acknowledge the generosity of the patients, who contributed time and effort to take part in this study.

Author Contributions:
Conceptualization: MWV
Experiments: RCC, ARC, PGG, CKK, AJG
Methodology: ARC, JFRV, MWV, CKK, HK
Data Analysis: ARC, JFRV
Visualization: ARC, JFRV, PGG
Funding acquisition: MAHIII, JDG
Supervision: MWV, MB, KVN
Writing – original draft: ARC, JFRV, MWV
Writing – review & editing: ARC, JFRV, MWV, MB, KVN, CKK, RCC, PGG, JDG

Competing interests: The authors declare that they have no competing interests.

Supplementary Materials

Materials and Methods

Table S1

References

1. M. Roig, S. Nordbrandt, S. S. Geertsen, J. B. Nielsen, The effects of cardiovascular exercise on human memory: a review with meta-analysis. *Neurosci. Biobehav. Rev.* **37**, 1645–1666 (2013).

2. T. Hatchard, J. J. Ting, C. Messier, Translating the impact of exercise on cognition: Methodological issues in animal research. *Behav. Brain Res.* **273**, 177–188 (2014).

3. C. Vivar, B. D. Peterson, H. van Praag, Running rewires the neuronal network of adult-born dentate granule cells. *NeuroImage*. **131**, 29–41 (2016).

4. M. W. Voss, C. Soto, S. Yoo, M. Sodoma, C. Vivar, H. van Praag, Exercise and Hippocampal Memory Systems. *Trends Cogn. Sci.* **23**, 318–333 (2019).

5. H. van Praag, B. R. Christie, T. J. Sejnowski, F. H. Gage, Running enhances neurogenesis, learning, and long-term potentiation in mice. *Proc. Natl. Acad. Sci. U. S. A.* **96**, 13427–13431 (1999).

6. J. Farmer, X. Zhao, H. van Praag, K. Wodtke, F. H. Gage, B. R. Christie, Effects of voluntary exercise on synaptic plasticity and gene expression in the dentate gyrus of adult male Sprague-Dawley rats in vivo. *Neuroscience*. **124**, 71–79 (2004).

7. A. T. Dao, M. A. Zagaar, A. T. Levine, K. A. Alkadhi, Comparison of the Effect of Exercise on Late-Phase LTP of the Dentate Gyrus and CA1 of Alzheimer's Disease Model. *Mol. Neurobiol.* **53**, 6859–6868 (2016).

8. T. B. Weng, G. L. Pierce, W. G. Darling, D. Falk, V. A. Magnotta, M. W. Voss, The Acute Effects of Aerobic Exercise on the Functional Connectivity of Human Brain Networks. *Brain Plast. Amst. Neth.* **2**, 171–190 (2017).

9. K. Suwabe, K. Byun, K. Hyodo, Z. M. Reagh, J. M. Roberts, A. Matsushita, K. Saotome, G. Ochi, T. Fukuie, K. Suzuki, Y. Sankai, M. A. Yassa, H. Soya, Rapid stimulation of human dentate gyrus function with acute mild exercise. *Proc. Natl. Acad. Sci.* **115**, 10487–10492 (2018).

10. M. W. Voss, R. S. Prakash, K. I. Erickson, C. Basak, L. Chaddock, J. S. Kim, H. Alves, S. Heo, A. N. Szabo, S. M. White, T. R. Wójcicki, E. L. Mailey, N. Gothe, E. A. Olson, E. McAuley, A. F. Kramer, Plasticity of Brain Networks in a Randomized Intervention Trial of Exercise Training in Older Adults. *Front. Aging Neurosci.* **2**, 32 (2010).

11. P. Flodin, L. S. Jonasson, K. Riklund, L. Nyberg, C. J. Boraxbekk, Does Aerobic Exercise Influence Intrinsic Brain Activity? An Aerobic Exercise Intervention among Healthy Old Adults. *Front. Aging Neurosci.* **9** (2017) (available at https://www.frontiersin.org/articles/10.3389/fnagi.2017.00267).

12. G. Buzsáki, Hippocampal sharp wave-ripple: A cognitive biomarker for episodic memory and planning. *Hippocampus*. **25**, 1073–1188 (2015).

13. G. Girardeau, K. Benchenane, S. I. Wiener, G. Buzsáki, M. B. Zugaro, Selective suppression of hippocampal ripples impairs spatial memory. *Nat. Neurosci.* **12**, 1222–1223 (2009).

14. I. Gridchyn, P. Schoenenberger, J. O'Neill, J. Csicsvari, Assembly-Specific Disruption of Hippocampal Replay Leads to Selective Memory Deficit. *Neuron*. **106**, 291-300.e6 (2020).

15. N. K. Logothetis, O. Eschenko, Y. Murayama, M. Augath, T. Steudel, H. C. Evrard, M. Besserve, A. Oeltermann, Hippocampal–cortical interaction during periods of subcortical silence. *Nature*. **491**, 547–553 (2012).

16. J. F. Ramirez-Villegas, N. K. Logothetis, M. Besserve, Diversity of sharp-wave–ripple LFP signatures reveals differentiated brain-wide dynamical events. *Proc. Natl. Acad. Sci.* **112** (2015), doi:10.1073/pnas.1518257112.

17. B. Frauscher, N. von Ellenrieder, R. Zelmann, C. Rogers, D. K. Nguyen, P. Kahane, F. Dubeau, J. Gotman, High-Frequency Oscillations in the Normal Human Brain. *Ann. Neurol.* **84**, 374–385 (2018).

18. A. P. Vaz, S. K. Inati, N. Brunel, K. A. Zaghloul, Coupled ripple oscillations between the medial temporal lobe and neocortex retrieve human memory. *Science*. **363**, 975–978 (2019).

19. Y. Norman, E. M. Yeagle, S. Khuvis, M. Harel, A. D. Mehta, R. Malach, Hippocampal sharp-wave ripples linked to visual episodic recollection in humans. *Science*. **365** (2019), doi:10.1126/science.aax1030.

20. D. Khodagholy, J. N. Gelinas, G. Buzsáki, Learning-enhanced coupling between ripple oscillations in association cortices and hippocampus. *Science*. **358**, 369–372 (2017).

21. G. Arnulfo, S. H. Wang, V. Myrov, B. Toselli, J. Hirvonen, M. M. Fato, L. Nobili, F. Cardinale, A. Rubino, A. Zhigalov, S. Palva, J. M. Palva, Long-range phase synchronization of high-frequency oscillations in human cortex. *Nat. Commun.* **11**, 5363 (2020).

22. B. T. Thomas Yeo, F. M. Krienen, J. Sepulcre, M. R. Sabuncu, D. Lashkari, M. Hollinshead, J. L. Roffman, J. W. Smoller, L. Zöllei, J. R. Polimeni, B. Fischl, H. Liu, R. L. Buckner, The organization of the human cerebral cortex estimated by intrinsic functional connectivity. *J. Neurophysiol.* **106**, 1125–1165 (2011).

23. N. Axmacher, C. E. Elger, J. Fell, Ripples in the medial temporal lobe are relevant for human memory consolidation. *Brain*. **131**, 1806–1817 (2008).

24. J. J. Sakon, M. J. Kahana, Hippocampal ripples signal contextually mediated episodic recall. *Proc. Natl. Acad. Sci.* **119**, e2201657119 (2022).

25. R. Cox, T. Rüber, B. P. Staresina, J. Fell, Sharp Wave-Ripples in Human Amygdala and Their Coordination with Hippocampus during NREM Sleep. *Cereb. Cortex Commun.* **1**, tgaa051 (2020).

26. A. Fernández-Ruiz, A. Oliva, E. Fermino de Oliveira, F. Rocha-Almeida, D. Tingley, G. Buzsáki, Long-duration hippocampal sharp wave ripples improve memory. *Science*. **364**, 1082–1086 (2019).

27. O. Eschenko, W. Ramadan, M. Mölle, J. Born, S. J. Sara, Sustained increase in hippocampal sharp-wave ripple activity during slow-wave sleep after learning. *Learn. Mem.* **15**, 222–228 (2008).

28. C. K. Kovach, A Biased Look at Phase Locking: Brief Critical Review and Proposed Remedy. *IEEE Trans. Signal Process.* **65**, 4468–4480 (2017).

29. S. L. Cowen, D. T. Gray, J.-P. L. Wiegand, L. A. Schimanski, C. A. Barnes, Age-associated changes in waking hippocampal sharp-wave ripples. *Hippocampus*. **30**, 28–38 (2020).

30. C. W. Dickey, I. A. Verzhbinsky, X. Jiang, B. Q. Rosen, S. Kajfez, B. Stedelin, J. J. Shih, S. Ben-Haim, A. M. Raslan, E. N. Eskandar, J. Gonzalez-Martinez, S. S. Cash, E. Halgren, Widespread ripples synchronize human cortical activity during sleep, waking, and memory recall. *Proc. Natl. Acad. Sci.* **119**, e2107797119 (2022).

31. K. Kaefer, F. Stella, B. L. McNaughton, F. P. Battaglia, Replay, the default mode network and the cascaded memory systems model. *Nat. Rev. Neurosci.* **23**, 628–640 (2022).

32. G. Girardeau, V. Lopes-dos-Santos, Brain neural patterns and the memory function of sleep. *Science*. **374**, 560–564 (2021).

33. I. P. Riches, F. A. Wilson, M. W. Brown, The effects of visual stimulation and memory on neurons of the hippocampal formation and the neighboring parahippocampal gyrus and inferior temporal cortex of the primate. *J. Neurosci.* **11**, 1763–1779 (1991).

34. K. Tanaka, Inferotemporal cortex and higher visual functions. *Curr. Opin. Neurobiol.* **2**, 502–505 (1992).

35. M. P. Witter, P. A. Naber, T. van Haeften, W. C. M. Machielsen, S. A. R. B. Rombouts, F. Barkhof, P. Scheltens, F. H. Lopes da Silva, Cortico-hippocampal communication by way of parallel parahippocampal-subicular pathways. *Hippocampus*. **10**, 398–410 (2000).

36. J. Karimi Abadchi, M. Nazari-Ahangarkolaee, S. Gattas, E. Bermudez-Contreras, A. Luczak, B. L. McNaughton, M. H. Mohajerani, Spatiotemporal patterns of neocortical activity around hippocampal sharp-wave ripples. *eLife*. **9**, e51972 (2020).

37. J. J. Chrobak, G. Buzsáki, High-Frequency Oscillations in the Output Networks of the Hippocampal–Entorhinal Axis of the Freely Behaving Rat. *J. Neurosci.* **16**, 3056–3066 (1996).

38. N. Nitzan, S. McKenzie, P. Beed, D. F. English, S. Oldani, J. J. Tukker, G. Buzsáki, D. Schmitz, Propagation of hippocampal ripples to the neocortex by way of a subiculum-retrosplenial pathway. *Nat. Commun.* **11**, 1947 (2020).

39. Y. Isomura, A. Sirota, S. Özen, S. Montgomery, K. Mizuseki, D. A. Henze, G. Buzsáki, Integration and Segregation of Activity in Entorhinal-Hippocampal Subregions by Neocortical Slow Oscillations. *Neuron*. **52**, 871–882 (2006).

40. T. T. G. Hahn, J. M. McFarland, S. Berberich, B. Sakmann, M. R. Mehta, Spontaneous persistent activity in entorhinal cortex modulates cortico-hippocampal interaction in vivo. *Nat. Neurosci.* **15**, 1531–1538 (2012).

41. J. O'Neill, C. N. Boccara, F. Stella, P. Schoenenberger, J. Csicsvari, Superficial layers of the medial entorhinal cortex replay independently of the hippocampus. *Science*. **355**, 184–188 (2017).

42. A. Fernández-Ruiz, A. Oliva, G. A. Nagy, A. P. Maurer, A. Berényi, G. Buzsáki, Entorhinal-CA3 Dual-Input Control of Spike Timing in the Hippocampus by Theta-Gamma Coupling. *Neuron*. **93**, 1213-1226.e5 (2017).

43. R. Kaplan, M. H. Adhikari, R. Hindriks, D. Mantini, Y. Murayama, N. K. Logothetis, G. Deco, Hippocampal Sharp-Wave Ripples Influence Selective Activation of the Default Mode Network. *Curr. Biol.* **26**, 686–691 (2016).

44. C. Higgins, Y. Liu, D. Vidaurre, Z. Kurth-Nelson, R. Dolan, T. Behrens, M. Woolrich, Replay bursts in humans coincide with activation of the default mode and parietal alpha networks. *Neuron*. **109**, 882-893.e7 (2021).

45. D. Tingley, K. McClain, E. Kaya, J. Carpenter, G. Buzsáki, A metabolic function of the hippocampal sharp wave-ripple. *Nature*. **597**, 82–86 (2021).

46. A. Feinsinger, N. Pouratian, H. Ebadi, R. Adolphs, R. Andersen, M. S. Beauchamp, E. F. Chang, N. E. Crone, J. L. Collinger, I. Fried, A. Mamelak, M. Richardson, U. Rutishauser, S. A. Sheth, N. Suthana, N. Tandon, D. Yoshor, NIH Research Opportunities in Humans Consortium, Ethical commitments, principles, and practices guiding intracranial neuroscientific research in humans. *Neuron*. **110**, 188–194 (2022).

47. K. V. Nourski, M. A. Howard, Invasive recordings in the human auditory cortex. *Handb. Clin. Neurol.* **129**, 225–244 (2015).

48. M. A. Howard, I. O. Volkov, R. Mirsky, P. C. Garell, M. D. Noh, M. Granner, H. Damasio, M. Steinschneider, R. A. Reale, J. E. Hind, J. F. Brugge, Auditory cortex on the human posterior superior temporal gyrus. *J. Comp. Neurol.* **416**, 79–92 (2000).

49. C. G. Reddy, N. S. Dahdaleh, G. Albert, F. Chen, D. Hansen, K. Nourski, H. Kawasaki, H. Oya, M. A. Howard, *J. Neurosurg.*, in press, doi:10.3171/2009.7.JNS09404.

50. J. M. Tyszka, W. M. Pauli, In vivo delineation of subdivisions of the human amygdaloid complex in a high-resolution group template. *Hum. Brain Mapp.* **37**, 3979–3998 (2016).

51. B. B. Avants, C. L. Epstein, M. Grossman, J. C. Gee, Symmetric diffeomorphic image registration with cross-correlation: evaluating automated labeling of elderly and neurodegenerative brain. *Med. Image Anal.* **12**, 26–41 (2008).

52. C. Destrieux, B. Fischl, A. Dale, E. Halgren, Automatic parcellation of human cortical gyri and sulci using standard anatomical nomenclature. *NeuroImage*. **53**, 1–15 (2010).

53. C. Destrieux, L. M. Terrier, F. Andersson, S. A. Love, J.-P. Cottier, H. Duvernoy, S. Velut, K. Janot, I. Zemmoura, A practical guide for the identification of major sulcogyral structures of the human cortex. *Brain Struct. Funct.* **222**, 2001–2015 (2017).

54. C. K. Kovach, P. E. Gander, The demodulated band transform. *J. Neurosci. Methods*. **261**, 135–154 (2016).

55. Y. Norman, O. Raccah, S. Liu, J. Parvizi, R. Malach, Hippocampal ripples and their coordinated dialogue with the default mode network during recent and remote recollection. *Neuron*. **109**, 2767-2780.e5 (2021).

56. J. F. Ramirez-Villegas, M. Besserve, Y. Murayama, H. C. Evrard, A. Oeltermann, N. K. Logothetis, Coupling of hippocampal theta and ripples with pontogeniculooccipital waves. *Nature*. **589**, 96–102 (2021).

57. D. R. Brillinger, Estimation of the Second-Order Intensities of a Bivariate Stationary Point Process. *J. R. Stat. Soc. Ser. B Methodol.* **38**, 60–66 (1976).

Supplementary Materials

Materials and Methods

Participants

A total of 14 neurosurgical participants completed the acute exercise paradigm, all while being monitored for epileptic seizure localization with chronic intracranial ECoG

recordings. Patient demographics and seizure onset zone are described in Table 1. Research protocols aligned with best practices recently aggregated in Feinsinger et al. (*46*). The University of Iowa Human Subjects Review Board approved the research protocol and written informed consent was obtained from each subject before the study.

Acute Exercise Paradigm

Prior to the acute exercise paradigm, all participants were screened using the Physical Activity Readiness Questionnaire (PAR-Q, Canadian Society for Exercise Physiology). Weekly physical activity was also assessed using the Paffenbarger Physical Activity Questionnaire (PPAQ). After a first rest period of approximately 20 minutes, participants had a guided exercise session on a MagneTrainer-ER mini-bike (MagneTrainer) placed on the ground beside their bed or at the foot of a chair next to the bed. This session was followed again by a post-exercise rest period of similar duration.

During rest periods, participants were instructed to relax with their eyes closed and avoid talking. In the exercise session, participants started with a 5-minute warm-up and then cycled at a light-to-moderate intensity of 50-60% of their age-predicted maximum heart rate (HR). Participants were given their target HR zone, so that they could monitor their pacing and adjust effort as needed. At the start of the warm-up period, bike resistance was set to half of the maximum resistance, and all participants were asked to start pedaling at a rate of 15 mph. Resistance was then adjusted until reaching a level that increased HR to the target HR zone and which the participants thought they could maintain for 20 minutes. Ratings of perceived exertion (RPE 6-20) were recorded following the warm-up and at 10-minute increments during exercise. The ECG read-out for HR was manually recorded by the experimenter at the start of the pre- and post-exercise rest periods.

Recording of iEEG data

Recordings were made using subdural and depth electrodes, manufactured by PMT Corporation, Chanhassen, MN (participant R348) or Ad-Tech Medical, Racine, WI (all other participants). All electrodes were placed solely on the basis of clinical requirements, as determined by a team of epileptologists and neurosurgeons (*47*). Details of electrode

implantation, recording and iEEG data analysis have been previously described in detail (*47–49*). In brief, subdural arrays consisted of platinum-iridium discs (2.3 mm diameter, 5–10 mm inter-electrode distance), embedded in a silicon membrane. These arrays provided coverage of frontal, parietal, temporal, and occipital cortex over the convexity of the cerebral hemispheres. Depth arrays (8–12 electrodes, 5 mm inter-electrode distance) targeted amygdala, hippocampus, cingulate, insular cortex and the superior temporal plane. A subgaleal electrode, placed over the cranial vertex near midline, was used as a reference in all participants.

In participants L275 through L348 data acquisition was controlled by a TDT RZ2 real-time processor (Tucker-Davis Technologies, Alachua, FL); in L399 through L457 data acquisition was performed using a Neuralynx Atlas System (Neuralynx, Bozeman, MT). Recorded data were amplified, filtered (0.1–500 Hz bandpass, 5 dB/octave rolloff for TDT-recorded data; 0.7–800 Hz bandpass, 12 dB/octave rolloff for Neuralynx-recorded data), digitized at a sampling rate of 2034.5 Hz (TDT) or 2000 Hz (Neuralynx) and stored for subsequent offline analysis.

Anatomical reconstruction and ROI parcellation

All patients underwent whole-brain high-resolution T1-weighted structural magnetic resonance imaging (MRI) scans ($1mm^3$ isotropic resolution) before electrode implantation. After electrode implantation, patients underwent MRI and thin-slice volumetric computerized tomography (CT) scans ($1mm^3$ isotropic resolution). Locations of the depth and subdural electrode contacts were extracted from post-implantation MRI and CT scans, based on localized magnetic susceptibility artifacts and metallic hyperdensities, respectively. Anatomical locations estimated from postoperative scans were then projected onto preoperative MRI scans using non-linear three-dimensional thin-plate spline warping to account for geometric distortions, guided by manually selected control points throughout each individual brain (typically numbering 50-100) until satisfactory alignment was achieved, with a target residual displacement no greater than 2-3 mm. Data across participants were pooled by transforming the electrode locations into a standard coordinate space referenced to the Montreal Neurological Institute (MNI) 152 template. This was done for each participant using automated volumetric nonlinear co-

registration to the MNI152 aligned CIT168 template brain (*50*). Volumetric co-registration used the ANTs software tool (*51*).

All recording sites were assigned an anatomical label based on the Destrieux atlas implemented as individualized and automated parcellation of cortical gyri using the Freesurfer software package (*52*, *53*). Further, all cortical recording sites were assigned a brain network label based on the Yeo7 network parcellation available in standard MNI space (*22*). For depth electrodes, anatomical assignment was informed by MRI sections along sagittal, coronal and axial planes, and review from the Neurosurgical team. (Table 1).

Signal Preprocessing

Recording sites in the SOZ and those exhibiting epileptiform activity (seizure or interictal) at any time during the recording were excluded. Channels were further rejected if they exhibited voltage values exceeding 5 standard deviations in more than 5% of the samples. Remaining LFP signals were denoised using the demodulated band transform (DBT) method (*54*). To deal with high frequency noise common across channels we applied SVD (singular value decomposition) to the high-pass (250 Hz) filtered signals of all recorded channels and the first component was further extracted.

Ripple detection

For the purpose of ripple detection, LFP signals were bipolar-referenced to white matter (*19*, *55*). White-matter (WM) signals were visually inspected to guarantee they did not exhibit pathological activity or residual noise. Mesial channels (HC, AMY and PHG) were re-referenced to the closest viable WM contact, preferentially in the same strip or electrode. Signals from other brain areas were re-referenced to an average signal calculated from non-mesial WM sites. Crucially, the WM channels used for HC re-referencing were not used to re-reference other signals. After re-referencing, LFP signals were filtered in the human ripple (70–160 Hz) frequency band (*19*, *23*) with a 4th order infinite-impulse response (IIR) Butterworth filter. This band-limited signal was then rectified, filtered below 25 Hz and Z-scored. Candidate events were detected as epochs exceeding a threshold proportional to the standard deviation of the signal, calculated

including the pre and post-exercise periods (4 SD in this case). When the instantaneous power of the z-scored signal exceeded 20 SD, events were considered noise and were discarded.

Ripple features

Three distinct features were computed for all detected ripple episodes (rate, duration and peak frequency). First, the rate estimate was computed as the total number of ripple events over the total recording time of each resting behavioral epoch (pre- or post-exercise). In addition, ripple duration was computed as the full-width at half-maximum of the peri-event filtered (70-160 Hz) and rectified LFP signal.

Statistical coupling between ripple time stamps

We estimated the statistical coupling between ripple events detected individually from hippocampal and cortical iEEG signals. For that purpose, we defined hippocampal-cortical channel pairs using one 'anchor' hippocampal site per subject. When more than one HC site was viable, anatomical location was used as selection criteria. Specifically, HC sites contralateral to the SOZ and putatively closer to CA1/CA3 were preferred (*16*, *19*, *56*).

Following (*57*) we obtained a histogram-type estimate of the cross-correlation functions of the (bivariate) point-processes corresponding to paired event types. For a set of ripple events occurring in the interval [0,*T*] of type $S=\{s_1,s_2,\ldots,s_n\}$ and type $K=\{t_1,t_2,\ldots,t_m\}$, the cross-correlation estimates are based on counts in the following set:

$$W_{SK}(u) = \{(j,k)|u-\beta < s_j - t_k < u+\beta\}, \ \ \forall \ s_j \neq t_k$$

$$J_{SK}(u) = \sum_{j,k} \begin{cases} 1 & (j,k) \in W_{SK} \\ 0 & otherwise \end{cases},$$

where 2β and *u* correspond to the histogram bin size and the center of the bin. Using $J_{SK}(.)$, we get the rate of coinciding events (in events/s) for a single experiment block as follows:

$$p_{SK}(u) = \frac{J_{SK}(u)}{T}$$

Statistical testing for the significance of the ripple coupling between areas was assessed by generating null-hypothesis distributions of the cross-correlation values in the time

window of ±250ms around zero lag. These correlation values were computed from 400-point processes of the same rate, drawn at random from a uniform distribution. The ground-truth cross-correlation values were then compared with that of the null-hypothesis distributions, from which a *p*-value was computed (*56*). Correlation values of $p<0.01$ were considered statistically significant. For the group-level statistical analysis (LME model), to avoid effects induced by baseline correlation values, cross-correlograms were baseline-corrected using the average of the above null-hypothesis distribution across time lags.

<u>Amplitude-weighted phase locking (awPLV) analysis</u>

Amplitude-weighted phase locking (awPLV) is an estimate based on the cross-spectrum S_{xy} between two signals *x* and *y*. In order to factor out the influence of amplitude covariance, the cross spectrum is normalized with $\int [A_X(t)A_Y(t)]dt$, where A_X(t) and A_Y(t) correspond to the instantaneous amplitudes of the signals *x* and *y* in a time window around the event occurrence. This normalization results in a weighted-average phase coherence (hence the name "amplitude-weighted"):

$$\widehat{\Upsilon_{XY}} = \sum_t w_t e^{\Delta\phi_{XY}(t)}$$

with weights w_t, given by:

$$w_t = \frac{A_X A_Y}{\sum_t A_X A_Y}$$

Like the standard PLV, the magnitude of this measure will be 1 if the signals *x* and *y* are perfectly phase locked, regardless of their amplitudes. In the absence of locking, the expected value of PLV is related to effective sample size (*28*). Thus, in order to compute pair-contact averages (here, across detected ripple events), effective sample size was approximated as:

$$\upsilon = \frac{(\sum_t w_t)^2}{\sum_t w_t^2}$$

with sample bias:

$$\epsilon = {}^{1}/_{\sqrt{\upsilon}}$$

Therefore, the sample bias-corrected awPLV measure writes:

$$\widehat{|\Upsilon_{XY}^{*}|} = \frac{\widehat{|\Upsilon_{XY}|} - \epsilon}{1 - \epsilon}$$

Spectral estimates of this analysis were performed using the demodulated band transform (DBT) across mesial-cortical contact pairs for frequency values below 200 Hz. As for the coupling (cross-correlation) analysis, we used one 'anchor' hippocampal contact per subject. Peri-ripple magnitude awPLV was computed in a time window of ±250 ms around the occurrence of hippocampal ripples to account for the trade-off between spectral and temporal resolution of the spectral estimate (*54*). Estimates of awPLV across detected events were then averaged. Finally, an average of the resulting awPLV in the ripple frequency band (70-160 Hz) per channel pair was then used for further statistical analysis across brain regions and subjects (see Mixed-effects statistical model). Only for visualization purposes in Fig. 4B, sample bias-corrected awPLV was computed using complex Morlet-wavelet time-frequency spectrograms.

<u>Linear Mixed Effects (LME) Models</u>

Effects of exercise on ripple features, ripple coupling, and peri-ripple awPLV were examined separately. Each model included experimental epoch (pre-, post-exercise) and anatomical region of interest (ROI) entered as within-subject factors. Random effects included an intercept and epoch effect (slope) modeled by subject ID (1 + epoch | SubjectID) and channel ID nested within subject ID (1 + epoch | SubjectID:ChanID), which accounted for variability unique to participants and their specific recording montage. Fixed effects of interest included the interaction between epoch and ROI for each level of the ROI factor (e.g., epoch:ROI interaction). Statistical significance was determined based on an interaction term having a p-value of $p<0.05$ within each model. In the mesial temporal parcellation, we defined three anatomical ROIs: HC, AMY, and PHG. For the neocortical parcellation we used seven canonical networks (*22*): Visual (VIS), Somatomotor (SM), Dorsal Attention (DAT), Ventral Attention (VAT), Limbic (LIM), Frontoparietal (FP), Default-mode network (DMN).

Patient	Age	Sex	Seizure focus	Avg HR (% max)
275	30	M	L ITG including PHG	62
287	18	M	R parietal med	59
292	50	F	L ant mesial temporal	59
294	18	M	R frontal ant	45
307	29	M	L insula lesion	52
322	28	F	R frontal ant	54
329	20	M	R orbitofrontal	56
335	33	M	L mesial temporal	62
348	17	M	R sup and mid temporal	60
399	22	F	R superior temporal	51
405	19	M	L frontal	68
416	32	M	L temporal (fusiform, lingual)	59
418	25	F	R temporoparietal	59
457	18	M	L mesial temporal	62
N	**14**	**10 M**		**14**
Median	**23.5**			**59**
Range	**17-50**			**45-68**

Table S1.

Patient Demographics. Patient experimental IDs (N=14), accompanied by their age (median and range are provided at the bottom of the table); sex (M: Masculine; F: Feminine; 4 females, 10 males); hippocampal electrode coverage (check symbol indicates HC coverage; n=10); hemisphere (R: right; L: left), and anatomical location of the seizure onset zone; and average heart rate as a percentage of the maximum (median and range are provided at the bottom of the table). PHG: Parahippocampal gyrus; ITG: Inferior temporal gyrus.